

RESEARCH

Open Access



# Bio-SS-TS as a Targeted Antitumor Drug Exerts an Anti-Liver Cancer Effect by Enhancing Mitochondria-Dependent Apoptosis

Jian Li<sup>1†</sup>, Yuanhua Qin<sup>2†</sup>, Mengjuan Li<sup>2</sup>, Jingli Shang<sup>2</sup>, Hang Chen<sup>2</sup>, Yadi Liu<sup>2</sup>, Bingjie Liu<sup>2</sup>, Pingxin Zhou<sup>2</sup>, Tiesuo Zhao<sup>2</sup>, Ge Wang<sup>2</sup>, Chunpo Ge<sup>2</sup>, Yu Zhang<sup>2</sup>, Huijie Jia<sup>2\*</sup> and Feng Ren<sup>2,3,4\*</sup>

## Abstract

Developing targeted therapeutic drugs for liver cancer remains a significant scientific and clinical challenge. Previous research by the authors showed that taraxasterol (TS) can enhance the antitumor immune response of T-lymphocytes, inhibiting the growth of liver cancer cells both in vivo and in vitro. To improve the targeting ability and efficacy of TS, the authors synthesized a novel compound, Bio-SS-TS, which utilizes the high expression of biotin receptors on tumor cell membranes to link biotin to TS for increased targeting to hepatocellular carcinoma cells, and its disulfide bond can be specifically hydrolyzed by high - level glutathione (GSH) in tumor cells to release the active component TS. In vitro, Bio-SS-TS reduced liver cancer cell (HepG2 and Huh7) proliferation, impaired mitochondrial membrane potential, decreased intracellular GSH content in tumor cells, increased the reactive oxygen species level, and promoted the release of cytochrome c. Endogenous GSH in cancer cells reduced the disulfide bond in Bio-SS-TS, releasing active TS components. In vivo, treatment with Bio-SS-TS caused no significant change in mouse body weight and no toxicity to the main organs. The present study comprehensively demonstrates that Bio-SS-TS exerts a potent anti - liver cancer effect by enhancing mitochondria-dependent apoptosis, which may provide a new candidate for targeted liver cancer therapy.

**Keywords** Bio-SS-TS, Targeted antitumor drug, Liver cancer, Apoptosis

<sup>†</sup>Jian Li and Yuanhua Qin contributed equally to this work.

\*Correspondence:

Huijie Jia  
zhongziqu1115@163.com  
Feng Ren  
renfeng@xxmu.edu.cn

<sup>1</sup>Department of Pathology, The First Affiliated Hospital of Xinxiang Medical University, Xinxiang, Henan 453003, China

<sup>2</sup>School of Basic Medical Sciences, Xinxiang Medical University, Xinxiang, Henan 453003, China

<sup>3</sup>Henan International Joint Laboratory of Immunity and Targeted Therapy for Liver-Intestinal Tumors, Xinxiang Medical University, Xinxiang, Henan 453003, China

<sup>4</sup>Henan Research Center for Engineering Technology in Digestive Tract Tumor Immune Digital Decoding and Cell Therapy, Xinxiang Medical University, Xinxiang 453003, China

## Background

Liver cancer is a primary cause of cancer-related mortality worldwide [1], and ranks the third as regards incidence and fourth as regards mortality [2]. Liver cancer is particularly prevalent in China and is associated with poor clinical outcomes and low patient survival rates [3, 4]. Hepatocellular carcinoma (HCC), intrahepatic cholangiocarcinoma (ICC) and the ICC-HCC combination represent the three main types of liver cancer [5]. Although conventional therapies, including surgery, chemotherapy and combination therapy are sufficiently effective, there is a need for the identification of novel therapeutic targets and creating medications for the treatment of liver cancer [6, 7]. Recent advancements in the discovery of



natural compounds with anticancer capabilities have provided an opportunity to identify more effective treatments for liver cancer [8, 9]. Studies have shown that *Taraxacum mongolicum*, often referred to as dandelion, a traditional Chinese herbal remedy, exhibits potent therapeutic efficacy in the treatment of cancers, hepatitis and other disorders [10, 11]. Taraxasterol (TS), a natural product derived from *Taraxacum mongolicum*, has been found to possess effective physiological, pharmacological and biological activities [12–14]. A recent study by the authors using in liver cancer cell lines demonstrated that TS is potent in inducing apoptosis and, in addition, in suppressing cell proliferation by arresting the cell cycle, thus exhibiting a potent inhibitory anticancer effect; however, the low solubility and cellular uptake of TS limits its anticancer capacity in vivo [15].

In recent years, research efforts have been focused on altering the chemical composition of drugs to enhance their therapeutic efficacy and decrease associated side-effects. Biotin receptors are extensively expressed on the surface of several types of cancer cells [16, 17], providing an excellent avenue with which to increase drug uptake by biotin-conjugation and biotin receptor-mediated internalization [18]. The disulfide bond (-S-S-) is an essential group that plays a role in numerous chemical and biological substances, and exhibits potent responsiveness to endogenous thiols, such as glutathione (GSH) and thioredoxin [19, 20], which can break the disulfide bond. The levels of both intracellular GSH and thioredoxin levels are elevated in cancer cells [18, 21]. In particular, compared to normal cells, cancer cells have markedly higher intracellular GSH levels, thus rendering GSH a critical factor in the development of antitumor drug delivery systems [22, 23].

In an aim to improve drug uptake, targeted specificity and reduce potential toxicity, the present study combined TS, biotin as the transporter and a disulfide linker, and synthesized the novel compound, Bio-SS-TS. The present study evaluated the antitumor potency of Bio-SS-TS against HepG2 and Huh7 cancer cell viability in vitro and in the development of liver cancer in mice in vivo. In addition, the present study further explored the mechanisms of action of Bio-SS-TS.

## Materials and Methods

### Preparation of Bio-SS-TS

Each experiment, unless otherwise indicated, was conducted using oven-dried glassware. The method used to track reactions was thin-layer chromatography (TLC). For TLC,  $8 \pm 0.2 \mu\text{m}$  pre-coated glass plates (0.25 mm in size, MilliporeSigma, Burlington, Massachusetts) were used, and visualization was performed using UV fluorescence quenching (Beijing Inokai Technology Co., Ltd, Beijing, China),  $\text{KMnO}_4$  (Sigma-Aldrich, St. Louis,

Missouri) or phosphomolybdic acid staining. Chromatography was carried out using Huanghai silica gel (Huanghai Chemical Co., Ltd., China) with a particle size of 200 mesh. On a Bruker ADVANCE III 400 MHz spectrometer (Bruker Corporation, Billerica, Massachusetts),  $^1\text{H}$  NMR and  $^{13}\text{C}$  NMR spectra at room temperature were recorded. All additional compounds, unless otherwise specified, were acquired from reliable vendors, such as Adamas-beta (Adamas Reagents Co., Ltd., Shanghai, China), TCI (Tokyo Chemical Industry Co., Ltd., Tokyo, Japan), J&K (J&K Scientific Ltd., Beijing, China), Bide (Bide Pharmatech Ltd., Shanghai, China) and Yinuokai (Beijing InnoChem Science & Technology Co., Ltd., Beijing, China). Dry solvents were acquired commercially or dried by running them down an activated alumina column while compressing with argon.

A 25-ml reaction flask was charged with biotin (244 mg, 1 mM), EDC·HCl (1-Ethyl-3-(3-dimethylamino-propyl) carbodiimide hydrochloride), 286 mg, 1.5 mM), HOBT (1-Hydroxybenzotriazole, 202 mg, 1.5 mM) and DMF (N, N-Dimethylformamide, 3 ml). Bis (2-hydroxyethyl) disulfide (770 mg, 5 mM) and Et3N (Triethylamine, 1.4 ml) were added at 25°C. These reagents were brought from Shanghai Bide Pharmatech Ltd. and Beijing Inokai Technology Co., Ltd. Following stirring overnight at room temperature, the mixture was quenched with 5 ml  $\text{H}_2\text{O}$  and extracted with 20 ml  $\times 2$  DCM (Dichloromethane, Beijing Inokai Technology Co., Ltd, China). To obtain Bio-SS-OH (235.8 mg, 0.62 mM, 62%), the blended organic layers underwent brine washing, drying on sodium sulfate, filtering, rotary evaporation for concentration, and flash chromatography on silica gel for purification.

The TS used in the present study was obtained from Raffines Biotechnology Co., Ltd., with a purity  $\geq 99\%$  and no endotoxins. A 25 ml flame-dried flask was filled with TS (213 mg, 0.5 mM) and DCM (5 ml), supplemented with BTC (120 mg, 0.4 mM), and DMAP (4-Dimethylaminopyridine, 301 mg, 2.5 mM, 2 M in DCM, Beijing Inokai Technology Co., Ltd) was then gently added at 0°C. The flask was then chilled under nitrogen, at 0°C. The mixture was agitated for 12 h at room temperature. Following the addition of Bio-SS-OH (190 mg, 0.5 mM) and Et3N (0.7 ml, 5 mM), the mixture was left to stir at room temperature for 36 h. The addition of  $\text{H}_2\text{O}$  terminated the reaction. Subsequently, the organic layer was dried, filtered and concentrated after the mixture was extracted using DCM (20 ml  $\times 2$ ). To create Bio-SS-TS, the residue was cleaned using flash chromatography (206 mg, 0.247 mM, 49%).

### Cells and Cell Culture

HepG2 and Huh7 human liver cancer cells, and normal human hepatocyte cells (THLE-2) used in the present

study were obtained from The Cell Bank of Type Culture Collection of the Chinese Academy of Sciences. The HepG2 and Huh7 cells were cultured in DMEM supplemented with 10% fetal bovine serum (FBS, Shanghai Zhongqiao Xinzhou Biotechnology Co., Ltd.) at 37°C in a 5% CO<sub>2</sub> humidified atmosphere. The THLE-2 cells were grown in specific medium (CM-0833, Pricella). H22 mouse hepatoma cells were obtained from the Chinese Typical Culture Collection Center and maintained in RPMI-1640 medium with 10% FBS in a 5% CO<sub>2</sub> incubator at 37°C. Prior to delivery, each cell line was verified using short tandem repeat (STR) profiling, and their propagation period was < 6 months.

#### Cell Counting Kit-8 (CCK-8) Assay

After seeding  $2 \times 10^3$  cells/well in 96-well plates, the cells were kept in an incubator with 5% CO<sub>2</sub> at 37°C until they adhered to the well. The cells in the wells were then treated with TS or Bio-SS-TS at a final concentration of 20 μM, for 24, 48, 72, 96 and 120 h. Each well received 10 μl CCK-8 reagent (MedChemExpress (Monmouth Junction, NJ, USA)) after each time point, and the wells were incubated at 37°C for 2 h. Using a Molecular Devices microplate reader, the absorbance at 450 nm was measured, and the cell viability was calculated as per the manufacturer's instructions.

#### Establishment of a Mouse Subcutaneous Tumor Model

Eighteen male Kunming mice with body weights ranging from 18 to 20 g (6–8 weeks old) were obtained from Zhejiang Weitong Lihua Laboratory Animal Technology Co., Ltd. The mice were kept at  $25 \pm 2^\circ\text{C}$  in a pathogen-free environment with a 12 h light/dark cycle. Each mouse received a subcutaneous injection of H22 cells ( $2 \times 10^6$ ) into the right axilla. The mice were returned to their breeding cages to allow tumors to grow for 1 week to an approximate size with a diameter of 5 mm. The tumor-bearing mice were randomly divided into three groups as follows: (i) The control group, in which the mice were not administered any treatment; (ii) the TS group, in which the mice received 5 mg/kg TS daily by intragastric injection for 14 days; and (iii) the Bio-SS-TS group, in which the mice received 12 mg/kg Bio-SS-TS daily by intragastric injection for 14 days. An identical volume of 0.9% normal saline (NaCl) was administered to the control group. Preliminary tests were performed to determine the doses and treatment intervals. Every other day, the body weight and tumor size of the mice were recorded. When the humane endpoints of the animals were reached, the mice were euthanized. Cervical dislocation was used to euthanize the mice. The specific criteria for reaching the humane endpoints were as follows: (i) The tumor volume did not exceed the ethical limit of 2,000 mm<sup>3</sup>; (ii) a notable decrease in the body weight of the animals was

measured; (iii) the activity level and general condition of the animals were observed. A weight loss of 20% due to cancer was set as the threshold for euthanizing the mice. The animal experiments were approved by the Animal Care and Use Committee of Xinxiang Medical University, Xinxiang, China (XYLL-20210489).

#### Immunohistochemistry (IHC)

To monitor cancer cell proliferation, tumor tissue sections were prepared for IHC staining with Ki-67. The portions underwent treatments with xylene and ethanol to dewax and dry them, followed by antigen retrieval using a citrate solution in a microwave oven. Following an overnight incubation at 4°C with a Ki-67 monoclonal antibody (1:2,000; Cat. No. 23709-1, Proteintech Group, Inc.), the sections were blocked with 1% BSA (Gibco; Thermo Fisher Scientific, Inc.). After staining with DAB and treating the sections with an HRP-conjugated secondary anti-rabbit IgG antibody (1:1,000; ZSGB-BIO, Cat. No. SP-9001), the sections were rinsed in PBS. Ultimately, the sections underwent hematoxylin counterstaining (Beyotime, C0107) at room temperature for 1 min. The hydrochloric acid-alcohol differentiation solution was prepared by mixing 75% ethanol and concentrated hydrochloric acid in a ratio of 100:1 and stored at room temperature. Then the sections were separated using alcohol and hydrochloric acid, and sealed with neutral resin glue (Beyotime, C0173). The stained sections were then scanned and images captured using an optical microscope with a camera (Nikon Corporation, Japan). The Ki-67 expression in tumor tissues was analyzed using ImageJ (version 1.4.3.67) software (National Institutes of Health) to assess the effects of treatment with TS and Bio-SS-TS on cancer cell proliferation.

#### Hematoxylin and Eosin (H&E) Staining

The slides are dewaxed and hydrated in a series of ethanol solutions prior to being stained with hematoxylin (Beyotime, C0105S) at room temperature for 2–5 min, which binds to nuclei and gives them a blue color. The slides were washed with water and differentiated in hydrochloric acid alcohol to remove excess dye and highlight the contrast between the nuclei and cytoplasm. The slides were rinsed in water and counterstained with eosin, which stains the cytoplasm and extracellular matrix with pink colour. The slides were washed with water to remove excess dye before sealed with neutral resin sealant and examined under an optical microscope (Nikon Corporation, Japan).

#### Colony Formation Assay

For this assay, six-well plates were seeded with  $2 \times 10^3$  cells per well, and the plates were incubated at 37°C with 5% CO<sub>2</sub>. After the cells adhered to the well, 20 μM

TS or Bio-SS-TS were added to the wells. The cells were examined daily, with the medium changed every 2 days. Once the cells formed clusters, following the removal of the media and two PBS washes, the cells were fixed for 30 min at room temperature with 4% paraformaldehyde (Beyotime, P0099). The fixed cells were stained at room temperature for 15 min with crystal violet dye (Beyotime, C0121, ready-to-use) before being cleaned on an ultra-pure water-based plate. The plate was inverted, and a mesh-covered transparent film was positioned on top of it. The number of colonies with > 10 cells was determined using a Nikon microscope (ECLIPSE Ts2R-FL, Nikon Corporation). Finally, the colony formation was calculated by colony number/inoculated cells  $\times 100\%$ .

#### Apoptosis Assay

A total of  $5 \times 10^4$  HepG2 or Huh7 cells per well were seeded in six-well plates and treated with 20  $\mu\text{M}$  Bio-SS-TS or TS for 72 h. Subsequently,  $5 \times 10^5$  cells were gathered and resuspended in 100  $\mu\text{l}$  FITC-V buffer (DOJINDO, AD10, Japan). Following this, 5  $\mu\text{l}$  V-FITC solution (DOJINDO, AD10, Japan) and 5  $\mu\text{l}$  PI solution (DOJINDO, AD10, Japan) were added, and the cells were incubated for 15 min at room temperature in the dark. Using Flowjo7.6 software and a flow cytometer (Cytoflex, Beckman Coulter, Inc.), the proportion of apoptotic cells was determined.

#### Cell Cycle Assay

A total of  $5 \times 10^4$  Huh7 and HepG2 cells were cultured into 6-cm cell dishes, and after the cells were adherent, they were exposed to either 20  $\mu\text{M}$  TS or Bio-SS-TS for 72 h. The cells were gathered and preserved at 4°C in 75% ethanol for 12–24 h. Following fixation, the cells were cleared in PBS and incubated with 50  $\mu\text{g/ml}$  PI. To remove the RNA from the mixture and solely retain the DNA for analysis, RNase A (Beyotime, C1052) was introduced. Data acquisition and analysis were performed using flow cytometry and Software Flowjo7.6 (Cytoflex, Beckman Coulter, Inc.).

#### Western Blot Analysis

Proteins were isolated from HepG2 or Huh7 cells, after growing in a 6-well plate and treatment with 20  $\mu\text{M}$  Bio-SS-TS for 72 h, using RIPA buffer (Beijing Solarbio Science & Technology Co., Ltd.). Protein concentrations were measured using the BCA assay. Protein lysates were extracted from tumor tissue samples in the same manner. Proteins were transferred to PVDF membranes after being separated using 12% sodium dodecyl sulfate-polyacrylamide gel electrophoresis (SDS-PAGE). The membranes were blocked with 5% skim milk in TBST at room temperature on a shaker for two hours and incubated overnight at 4°C with primary rabbit antibodies against

$\alpha$ -tubulin (1:1,000; Cat. No. 66031-1-Ig, Proteintech Group, Inc.), caspase-3 (1:1,000; Cat. No. 19677-1-AP Proteintech Group, Inc.), Bax (1:1,000; Cat. No. 50599-2-Ig, Proteintech Group, Inc.) or cytochrome *c* (1:1,000; Cat. No. 11940, Cell Signaling Technology, Inc.). The membranes were incubated with the secondary goat anti-rabbit IgG antibody (CW Bio, CW0103S, diluted 1:10000 in milk) at room temperature for 45 min after being cleaned with TBST. Enhanced chemiluminescence was used for the visualization and quantification of proteins, using the Multifunctional Chemiluminescence Imaging System (Viliber).

#### Measurement of Mitochondrial Membrane Potential

Following the manufacturer's instructions, the mitochondrial membrane potential was monitored using JC-1 (C2006, Beyotime Institute of Biotechnology). The HepG2 and Huh7 cells were seeded in 6-well plates at the same density as that used for the apoptosis assay and treated with 20  $\mu\text{M}$  Bio-SS-TS for 72 h. After removing the culture medium, 1 ml fresh medium and 1 ml JC-1 staining solution were added in each well, and the cells were incubated at 37°C for 20 min. The media were then aspirated and the cells twice were washed with a staining buffer containing JC-1. The fluorescence was observed by the addition of 2 ml culture medium and observation using a Nikon fluorescence microscope (Nikon Corporation). For flow cytometric analysis, the HepG2 and Huh7 cells were exposed to 20  $\mu\text{M}$  Bio-SS-TS for 72 h, and 0.5 ml culture media were used to resuspend  $5 \times 10^5$  cells. After being combined with 0.5 ml JC-1 staining solution, the cells were incubated for 20 min in a tissue incubator. The cells were centrifuged for 4 min at 600  $\times g$  and 4°C following incubation. The cells were twice washed with JC-1 staining buffer after the supernatant was removed before re-suspended in JC-1 staining solution and examined with Flowjo V10 software.

#### GSH Content Assay

HepG2 and Huh7 cells were seeded in 10 cm culture dishes as described above. Following incubation with 20  $\mu\text{M}$  TS or Bio-SS-TS for 72 h, the cells were washed with PBS twice and digested with trypsin, and collected by centrifugation. After washing with PBS for two or more times, the cells were collected by low-speed centrifugation and again suspended in 0.3–0.5 ml of PBS buffer that is isotonic. The centrifugation conditions in this test were as follows: at 157  $\times g$ , for 3 min, and at room temperature. The cells were disrupted by ultrasonication, or manual grinding. A GSH assay kit was used to measure the GSH levels in accordance with the manufacturer's instructions (A006-2-1, Njjcbio).

### Ultrastructure Examination Using Transmission Electron Microscopy

The HepG2 cells were planted in 6-cm culture dishes with  $1 \times 10^6$  cells per well and allowed to grow overnight. Following treatment with 20  $\mu\text{M}$  Bio-SS-TS for 72 h, the cells were washed with PBS before being trypsinized; the cells were then collected by centrifugation with the condition: 157  $\times$ g, for 3 min at room temperature. After being fixed for 30 min at room temperature, away from light, the cells were re-suspended in 2.5% glutaraldehyde fixative solution and incubated at 4°C before transferred onto an ice pack from Servicebio Company for transmission electron microscopy detection.

### Detection of Intracellular Reactive Oxygen Species (ROS)

The HepG2 cells, prepared in 6-well plates and treated with 20  $\mu\text{M}$  Bio-SS-TS for 72 h as described above, were collected by trypsinization and centrifugation with the condition: 157  $\times$ g, for 3 min at room temperature. A total of  $5 \times 10^5 - 1 \times 10^6$  cells were gathered in 1.5-ml EP tubes, resuspended in 10  $\mu\text{M}$  of H2DCFDA diluted in serum-free DMEM, and incubated 37°C for 30 min. The cells were then washed three times with serum-free medium. ROS within cells were measured using a flow cytometer (Beckman Coulter, Inc.) and Flowjo V10 software.

### Safety-Testing Experiments

A total of 5 Kunming mice (6–8 weeks old) were randomly assigned to the control/saline group and four Bio-SS-TS treatment group: 2.5 mg/kg group, 5 mg/kg group, 10 mg/kg group, 20 mg/kg group. Apart from the different doses of the drug administered, the method of drug administration and other feeding conditions were the same as those aforementioned. The mice were treated via gavage on time every day for 14 consecutive days, and weighed every other day. On the last day, the blood collection for detecting blood biochemical indexes ([alanine transaminase (ALT), aspartate aminotransferase (AST), blood urea nitrogen (BUN) and, serum creatinine (SCR)]) was carried out by taking blood from the eyeballs of the mice prior to their euthanasia. After the blood collection, the mice were then euthanized. The livers, kidneys, heart, lung and brain were taken from the mice and weighed. These organs were placed into embedding cassettes, and fixed in paraformaldehyde for subsequent H&E staining.

### Statistical Analysis

The data are presented as the mean  $\pm$  SD, unless otherwise indicated. Each experiment was conducted at least three times. Differences between groups were examined using one-way ANOVA, followed by Tukey's HSD post hoc test. A value of  $P < 0.05$  was considered to indicate a statistically significant difference. The binding data were

examined using GraphPad Prism software (Graphpad Prism 6.01, Dotmatics).

## Results

### Spectral Data of Bio-SS-OH and Bio-SS-TS

Bio-SS-OH: 1 H NMR (400 MHz, D6-DMSO)  $\delta$ : 6.41 (d,  $J = 30.4$  Hz, 2 H), 4.92–4.89 (m, 1 H), 4.32–4.29 (m, 1 H), 4.25 (t,  $J = 6.4$  Hz, 2 H), 4.15–4.12 (m, 1 H), 3.64–3.59 (m, 2 H), 3.11–3.08 (m, 1 H), 2.96 (t,  $J = 6.4$  Hz, 2 H), 2.85–2.79 (m, 3 H), 2.58 (d,  $J = 12.4$  Hz, 1 H), 2.33–2.29 (m, 2 H), 1.63–1.29 (m, 6 H); 13 C NMR (100 MHz, D6-DMSO)  $\delta$ : 173.2, 163.2, 62.2, 61.5, 59.8, 55.6, 55.8, 41.5, 37.0, 33.7, 28.4, 24.9.

Bio-SS-TS: 1 H NMR (400 MHz, CDCl<sub>3</sub>)  $\delta$ : 5.74 (s, 1 H), 5.31 (s, 1 H), 4.62–4.60 (m, 2 H), 4.54–4.51 (m, 1 H), 4.39–4.32 (m, 6 H), 3.19–3.15 (m, 1 H), 2.98–2.93 (m, 5 H), 2.75 (d,  $J = 12.8$  Hz, 1 H), 2.43 (d,  $J = 10.4$  Hz, 1 H), 2.38–2.35 (m, 2 H), 2.23–2.16 (m, 1 H), 2.11–2.00 (m, 1 H), 1.74–0.085 (m, 49 H); 13 C NMR (100 MHz, CDCl<sub>3</sub>)  $\delta$ : 173.4, 163.1, 155.0, 154.6, 107.2, 85.8, 65.4, 62.1, 61.9, 60.1, 55.4, 55.3, 50.4, 48.6, 42.1, 40.9, 40.6, 39.4, 39.1, 38.9, 38.4, 38.3, 38.1, 37.3, 37.1, 37.0, 34.5, 34.0, 33.7, 28.3, 28.2, 27.9, 26.6, 26.1, 25.6, 25.5, 24.7, 23.7, 21.5, 19.5, 18.1, 16.5, 16.3, 15.9, 14.8; HRMS (ESI)  $m/z$ :  $[M + H]^+$  calcd for C<sub>45</sub>H<sub>73</sub>N<sub>2</sub>O<sub>6</sub>S<sub>3</sub> 833.4625; found 833.4598 (Fig. 1).

### Bio-SS-TS Inhibits Liver cancer Cell Proliferation

The viability and proliferation of HepG2 and Huh7 cells were assessed using the CCK-8 assay to investigate the effect of Bio-SS-TS on liver cancer cells after exposure to 20  $\mu\text{M}$  Bio-SS-TS for different durations, including 24, 48, 72, 96, and 120 h. The effects were compared with those of treatment with the parental TS at the same concentration. A potent and time-dependent suppression of cell growth and survival was observed in the HepG2 cells treated with Bio-SS-TS; this inhibition was comparable to that observed in the cells treated with TS (Fig. 2A and B). Similarly, Huh7 cells treated with Bio-SS-TS exhibited a significant time-dependent decrease in their ability to proliferate and survive; this suppression was comparable to that observed with TS (Fig. 2C and D). Subsequently, the present study assessed the effects of treatment with Bio-SS-TS or TS on the colony-forming ability of liver cancer cells. Colony formation was significantly inhibited when the HepG2 and Huh7 cells were treated with 20  $\mu\text{M}$  Bio-SS-TS or TS for 72 h (Fig. 2E–G). Collectively, these findings suggest that Bio-SS-TS, similar to TS, potently suppresses liver cancer cell proliferation.

### Bio-SS-TS Regulates the Progression of the Cell Cycle in Liver cancer Cells

In order to investigate the effects of Bio-SS-TS on the proliferation of liver cancer cells, flow cytometry was used to analyze the proportion of HepG2 and Huh7 cells

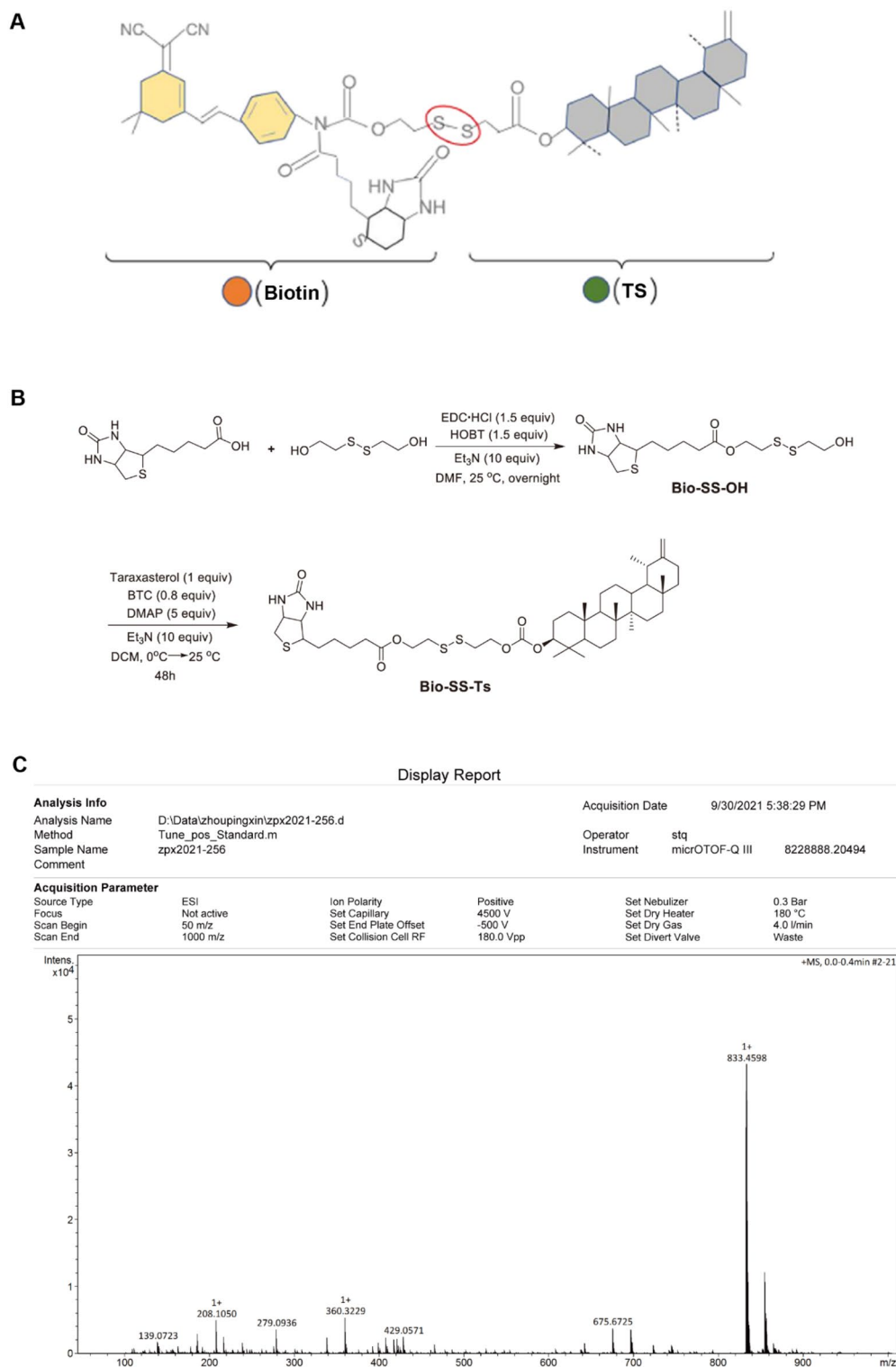


**Fig. 1** Synthesis of Bio-SS-TS. **A** Molecular structure of Bio-SS-TS. **B** Synthesis method for Bio-SS-TS. **C** HRMS spectrum of Bio-SS-TS

in various cell cycle phases. The HepG2 cells treated with 20  $\mu$ M Bio-SS-TS or TS for 72 h had a higher and lower percentage of cells in the G1 phase and S phase, respectively (Fig. 3A and B). Treatment of the Huh7

cells with Bio-SS-TS or TS also increased the cell population in the G1 phase and reduced the cell population in the G2 phase (Fig. 3C and D). In addition, western blot analysis was used to examine the expression of the

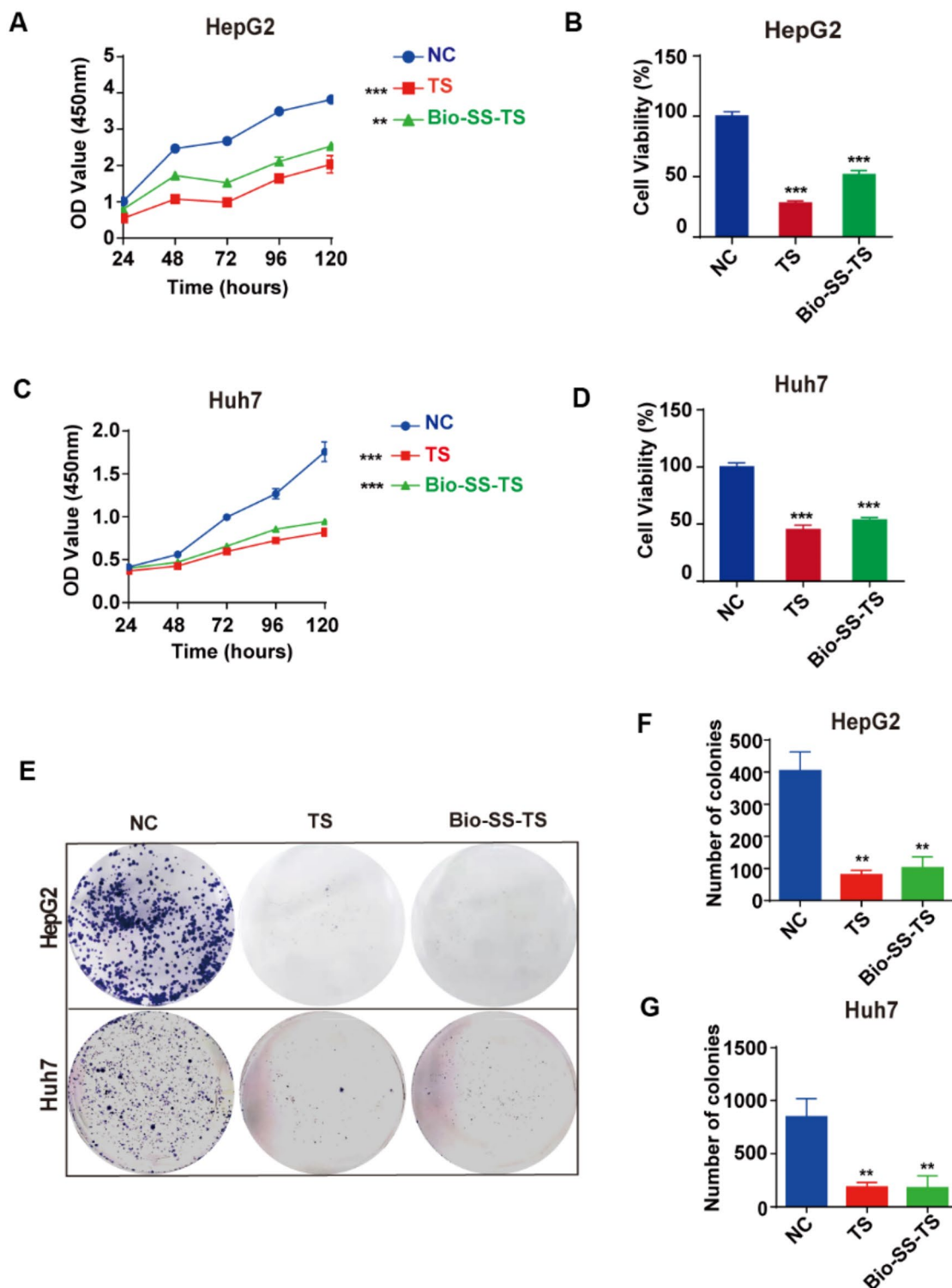


**Fig. 2** Bio-SS-TS significantly inhibited the proliferation of hepatoma cells in vitro. **A-D** We examined the effect of 20  $\mu$ M TS and Bio-SS-TS on the proliferation of HepG2/Huh7 cells at different time points (24, 48, 72, 96, and 120 h). **E-G** A plate clone formation assay was used to detect the effect of 20  $\mu$ M TS and 20  $\mu$ M Bio-SS-TS on the colony formation ability of HepG2/Huh7 cells. The results were obtained from tests performed in triplicate from at least three independent experiments. \*\* $P < 0.01$ ; \*\*\*  $P < 0.001$

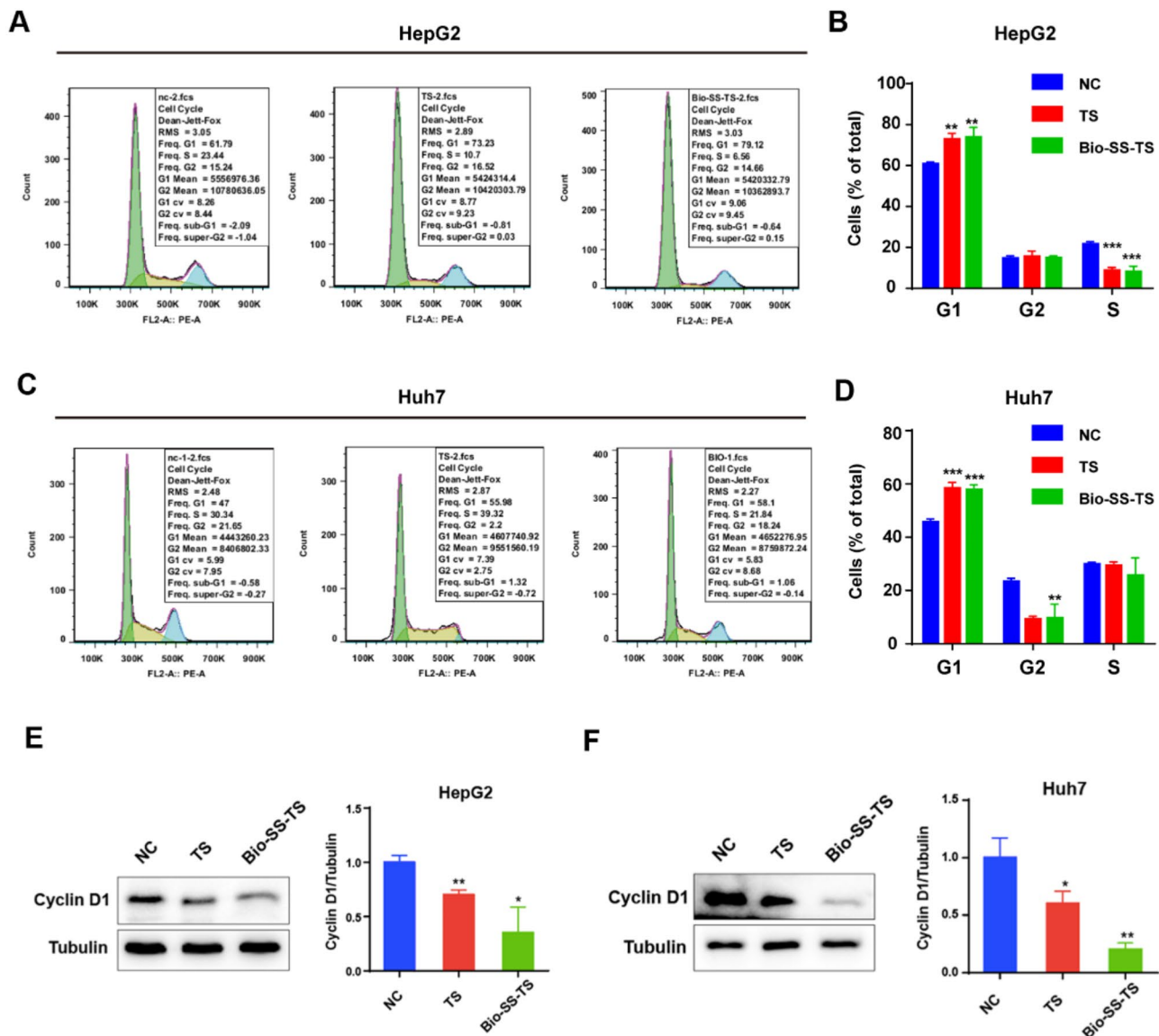


**Fig. 3** Bio-SS-TS arrested the cell cycle in vitro. **A-D** The effect of 20  $\mu$ M TS and 20  $\mu$ M Bio-SS-TS on the HepG2/Huh7 cell cycle was observed by propidium iodide staining. **E-F** The expression of Cyclin D1 was detected in HepG2/Huh7 cells. The results were obtained from tests performed in triplicate from at least three independent experiments. \*  $P < 0.05$ ; \*\*  $P < 0.01$ ; \*\*\*  $P < 0.001$

cell cycle-related protein, cyclin D1. Following treatment with Bio-SS-TS, the expression level of cyclin D1 in the HepG2 and Huh7 cells was significantly lower than that in the control cells (Fig. 3E and F). These results indicate that treatment with Bio-SS-TS inhibits liver cancer cell proliferation.

#### Bio-SS-TS Induces the Apoptosis of Liver Cancer Cells

Using flow cytometry in conjunction with Annexin V-FITC/PI double labeling, the capacity of Bio-SS-TS to induce the apoptosis of liver cancer cells was evaluated. Treatment of the HepG2 cells with Bio-SS-TS TS for 72 h promoted cell apoptosis (Fig. 4A). Similar results were observed in the Huh7 cells following treatment

with Bio-SS-TS or TS (Fig. 4B). These results, together with the results described above, indicate that Bio-SS-TS reduces liver cell viability by inducing apoptosis, as well as by inhibiting cell proliferation.

#### Bio-SS-TS Suppresses Liver Cancer Growth in Mice

To assess the inhibitory effects of Bio-SS-TS on liver cancer growth in vivo, using prior implanted H22 mouse liver cancer cells in mice, the present study first examined the effects of Bio-SS-TS treatment on the size and the mass of the tumors. Similar to TS, Bio-SS-TS significantly reduced the tumor volume and weight, indicating the inhibition of tumor growth by Bio-SS-TS in vivo (Fig. 5A-C). Following treatment with Bio-SS-TS or TS, western

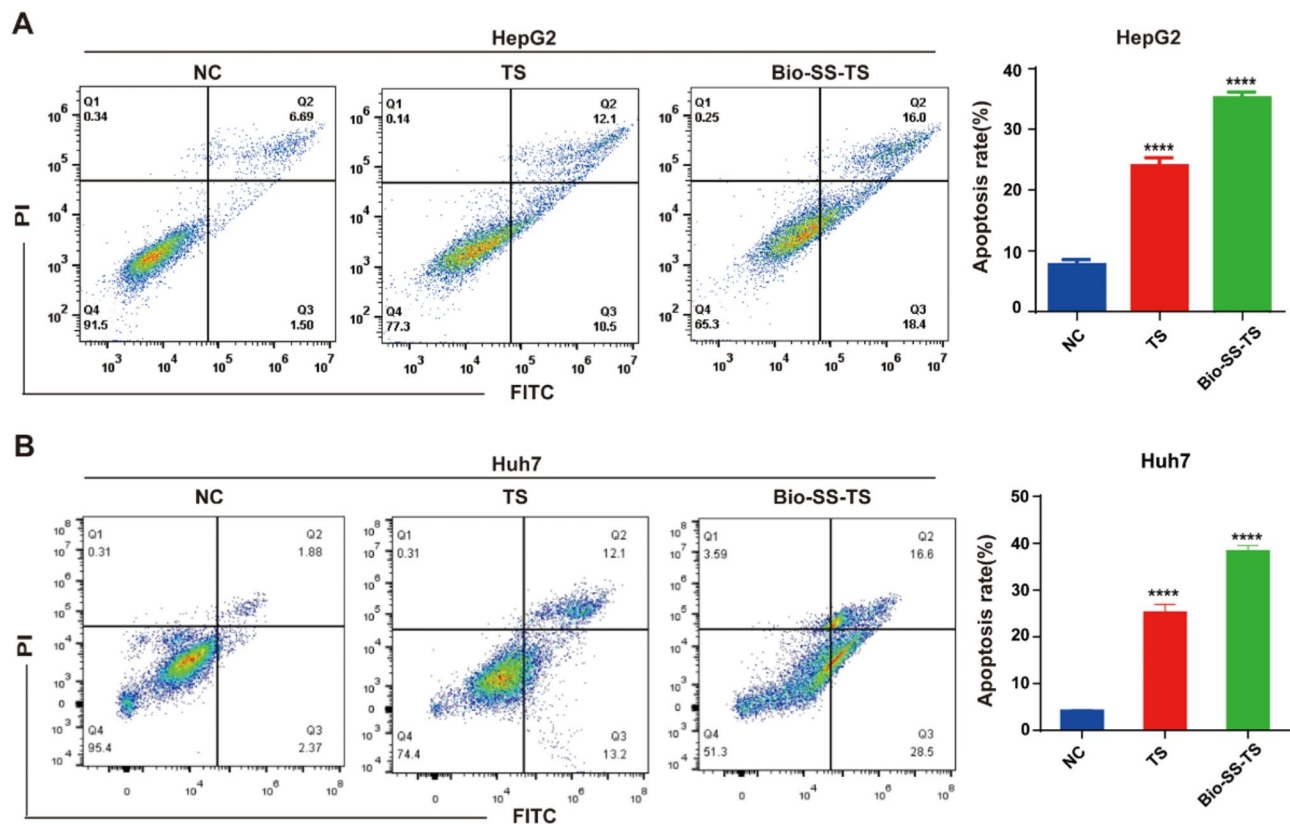


**Fig. 4** Bio-SS-TS induced apoptosis of hepatoma cells in vitro. **A-B** Annexin V/PI double staining was used to investigate the effect of treatment of HepG2 (A) and Huh7 cells (B) with 20  $\mu$ M Bio-SS-TS for 72 h on their apoptotic rates. The results were obtained from tests performed in triplicate from at least three independent experiments. \*  $P < 0.05$ ; \*\*  $P < 0.01$ ; \*\*\*  $P < 0.001$

blot analysis was also used to examine the expression of the apoptosis-related proteins, Bax and caspase-3, in the tumor tissues of the tumor-bearing mice (Fig. 5D). Consistent with the results obtained in vitro, treatment with Bio-SS-TS or TS and substantially increased the expression levels of caspase-3 and Bax in the tumor tissues. Furthermore, the present study assessed the effects of treatment with Bio-SS-TS or TS on cell proliferation by staining with the proliferation marker, Ki-67. The staining intensity of Ki-67 in the tumor tissues was significantly suppressed following treatment with Bio-SS-TS or TS (Fig. 5E). These results from the in vivo experiments provide further evidence to indicate that Bio-SS-TS significantly suppresses liver cancer growth by inducing liver cancer cell apoptosis and inhibiting liver cancer cell proliferation. Moreover, the present study further examined the infiltration of T-lymphocytes in the tumor tissues. The results revealed that Bio-SS-TS significantly increased the infiltration of CD4<sup>+</sup> and CD8<sup>+</sup> T-lymphocytes in the tumor tissues (Fig. S1).

#### Bio-SS-TS Has No Toxicity in Vivo

Finally, the safety of Bio-SS-TS was assessed by administering a range of doses (2.5, 5, 10 and 20 mg/kg) to

Kunming mice. The body weight of the mice treated with Bio-SS-TS did not exhibit any notable alterations (Fig. 6A). H&E staining of the tissue sections of major tissue and organs demonstrated that treatment with Bio-SS-TS had no significant effect on the liver, kidneys, heart, brain and lung (Fig. 6B and S2). The ALT, AST, BUN and SCR levels were unaffected by treatment with Bio-SS-TS at the concentrations used (Fig. 6C-F). In general, these results indicate that Bio-SS-TS is safe for application in vivo.

#### Bio-SS-TS Induces Mitochondrial Damage in Liver Cancer Cells

As demonstrated above that Bio-SS-TS induces liver cancer cell apoptosis, the mitochondrial ultrastructure was examined using transmission electron microscopy. In the HepG2 cells treated with 20  $\mu$ M Bio-SS-TS for 72 h, the majority of the mitochondria were elongated or dumbbell-shaped, and there was salient mitochondrial membrane damage with some of the outer and inner membranes vanished, resulting in a blurred structure, and, in addition, mitochondrial fusion (Fig. 7A).

We aimed to explore the impact of Bio-SS-TS on mitochondrial membrane potential and apoptosis in liver

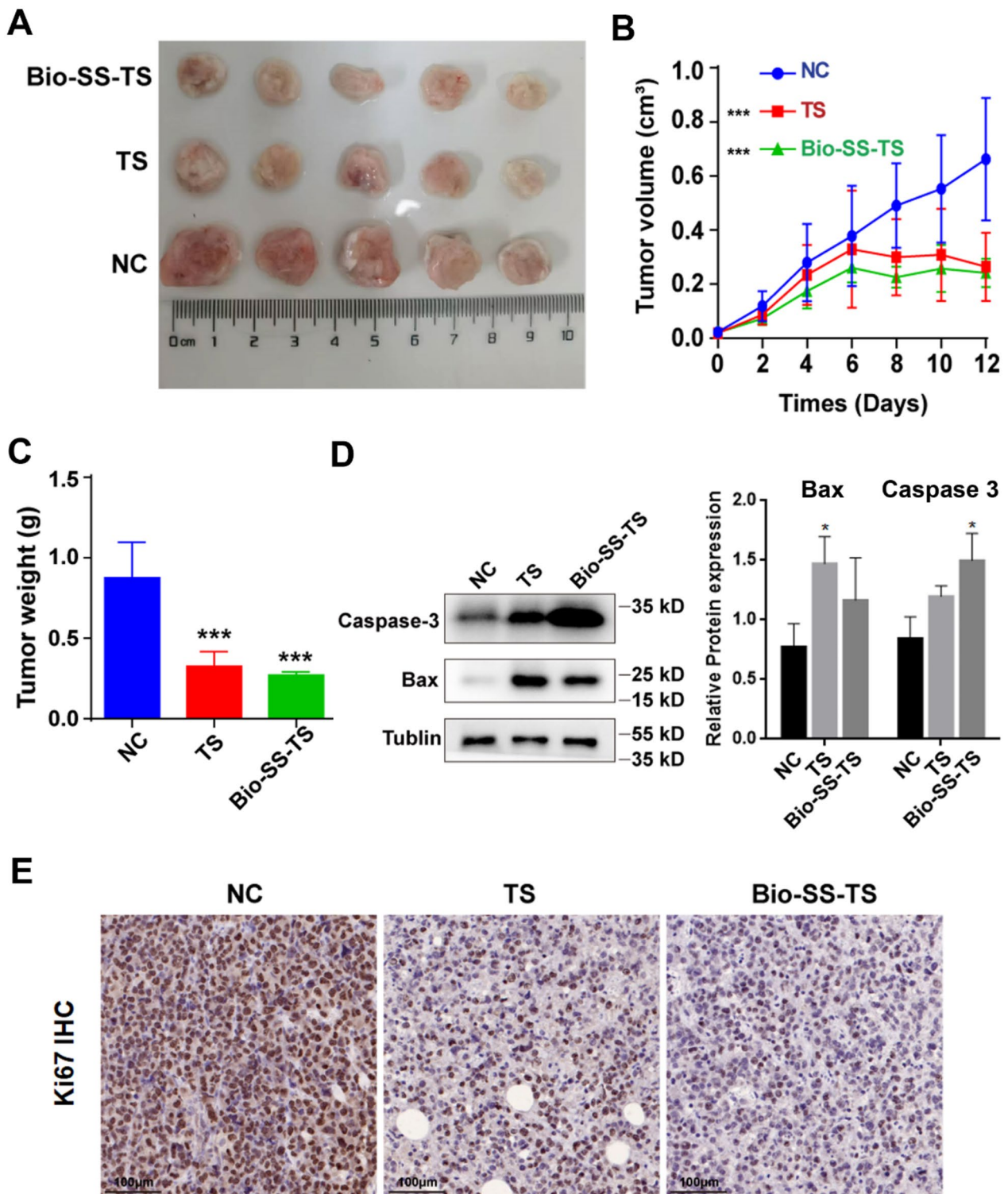


**Fig. 5** Bio-SS-TS inhibited tumor growth in H22 tumor-bearing mice in vivo. **A** The tumor images of H22-bearing mice. **B** Changes in tumor volume in H22-bearing mice. **C** Tumor weight of H22-bearing mice. **D** The expression levels of Bax and Caspase-3 proteins were detected in tumor tissues after treatment with TS and Bio-SS-TS. **E** Ki-67 proliferation was detected in tumor cells. \*\*\*  $P < 0.001$

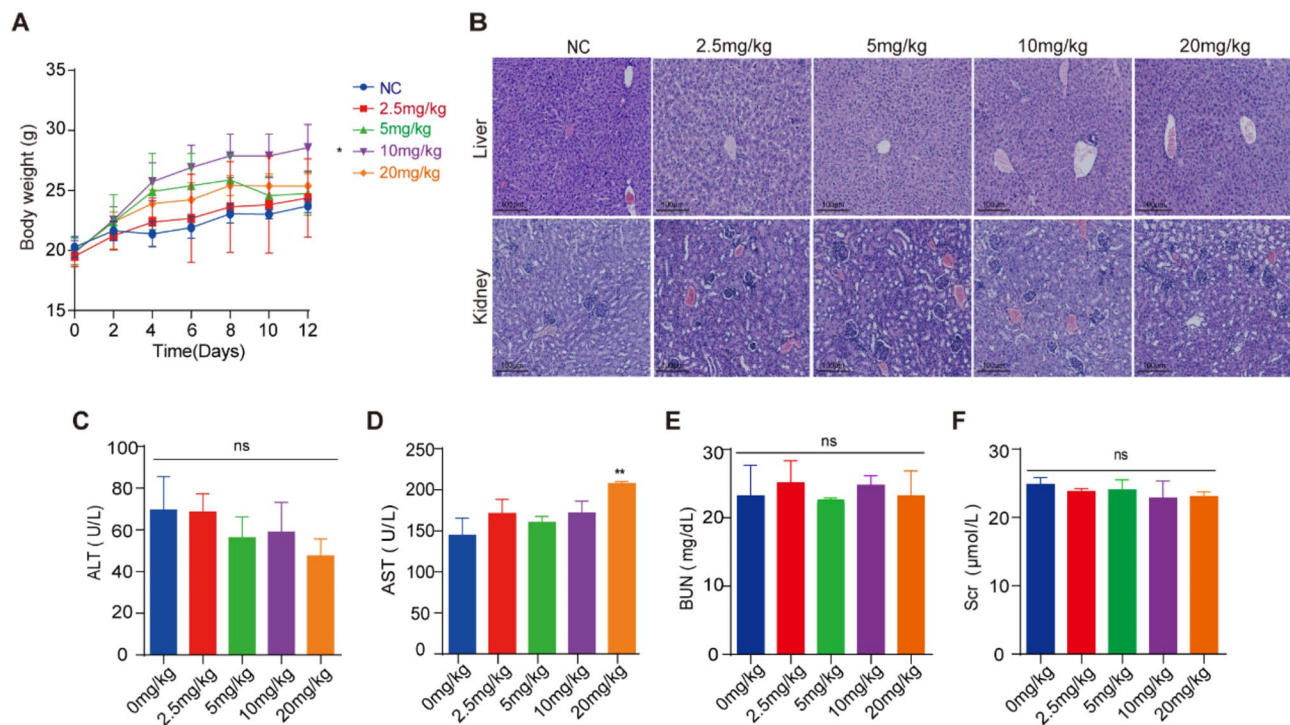


**Fig. 6** Safety of Bio-SS-TS in Living Organisms. **A** The effect of different concentrations of Bio-SS-TS (0, 2.5, 5, 10, and 20 mg/kg) on the body weight of Kunming mice was examined. **B** The effects of Bio-SS-TS on the liver and kidney of Kunming mice were examined using H&E staining. **C-F** The effects of different concentrations of Bio-SS-TS on serological indexes were detected by blood biochemical experiments. \*  $P < 0.05$ ; \*\*  $P < 0.01$

cancer cells. To serve as a positive control and better interpret mitochondrial-related changes, we employed CCCP (carbonyl cyanide 3-chlorophenylhydrazine), a well-recognized mitochondrial uncoupler. CCCP disrupts the mitochondrial membrane potential by enhancing the proton permeability of the inner mitochondrial membrane, which dissipates the proton electrochemical gradient, inhibits ATP synthesis, and triggers the release of cytochrome *c* from mitochondria, ultimately leading to apoptosis.

We treated liver cancer cells with Bio-SS-TS and a separate group with CCCP for 72 h. Subsequently, we used fluorescence microscopy combined with JC-1 labeling and flow cytometry to evaluate the effects of Bio-SS-TS on the mitochondrial membrane potential of HepG2 and Huh7 cells.

As shown in Fig. 7B, after 72-hour treatment with 20  $\mu$ M Bio-SS-TS, HepG2 and Huh7 cells showed an increase in green fluorescence (JC1 monomers), which indicates a decrease in mitochondrial membrane potential. Flow cytometry results further confirmed these findings. Both HepG2 (Fig. 7C) and Huh7 cells (Fig. S3) displayed a significant rise in the green fluorescence intensity of JC-1 compared to the control group. These results collectively suggest that Bio-SS-TS reduces mitochondrial membrane potential and impairs the integrity of mitochondrial membranes in liver cancer cells.

#### Bio-SS-TS Reduces Intracellular GSH and ROS Levels

As aforementioned, in cancer cells, the intracellular GSH level is increased. Thus, the present study assessed the intracellular GSH content in both normal THLE-2 liver cells and HepG2 and Huh7 cells. As was expected, the HepG2 and Huh7 cells exhibited markedly higher intracellular GSH levels than the THLE-2 normal liver cells (Fig. 8A). GSH is known to break disulfide bonds, thereby resulting in a reduction in the GSH level. The intracellular GSH levels were also evaluated in the HepG2 and Huh7 cells treated with Bio-SS-TS for 72 h. The intracellular GSH levels were significantly lower in the Bio-SS-TS-treated cells than in the control cells (Fig. 8B and C).

As aforementioned, treatment with Bio-SS-TS caused damage to mitochondrial membrane potential. Thus, the present study also examined whether Bio-SS-TS affects the ROS levels in cells. The intracellular ROS level was found to be substantially higher in the Bio-SS-TS-treated HepG2 and Huh7 cells than in the control cells (Fig. 8D and E). Lastly, western blot analysis was used to examine the expression of cytochrome *c*, caspase-3 and Bax. The Bax, caspase-3 and cytochrome *c* levels in the Bio-SS-TS-treated HepG2 and Huh7 cells were markedly higher than those in the control cells (Fig. 8F and G).

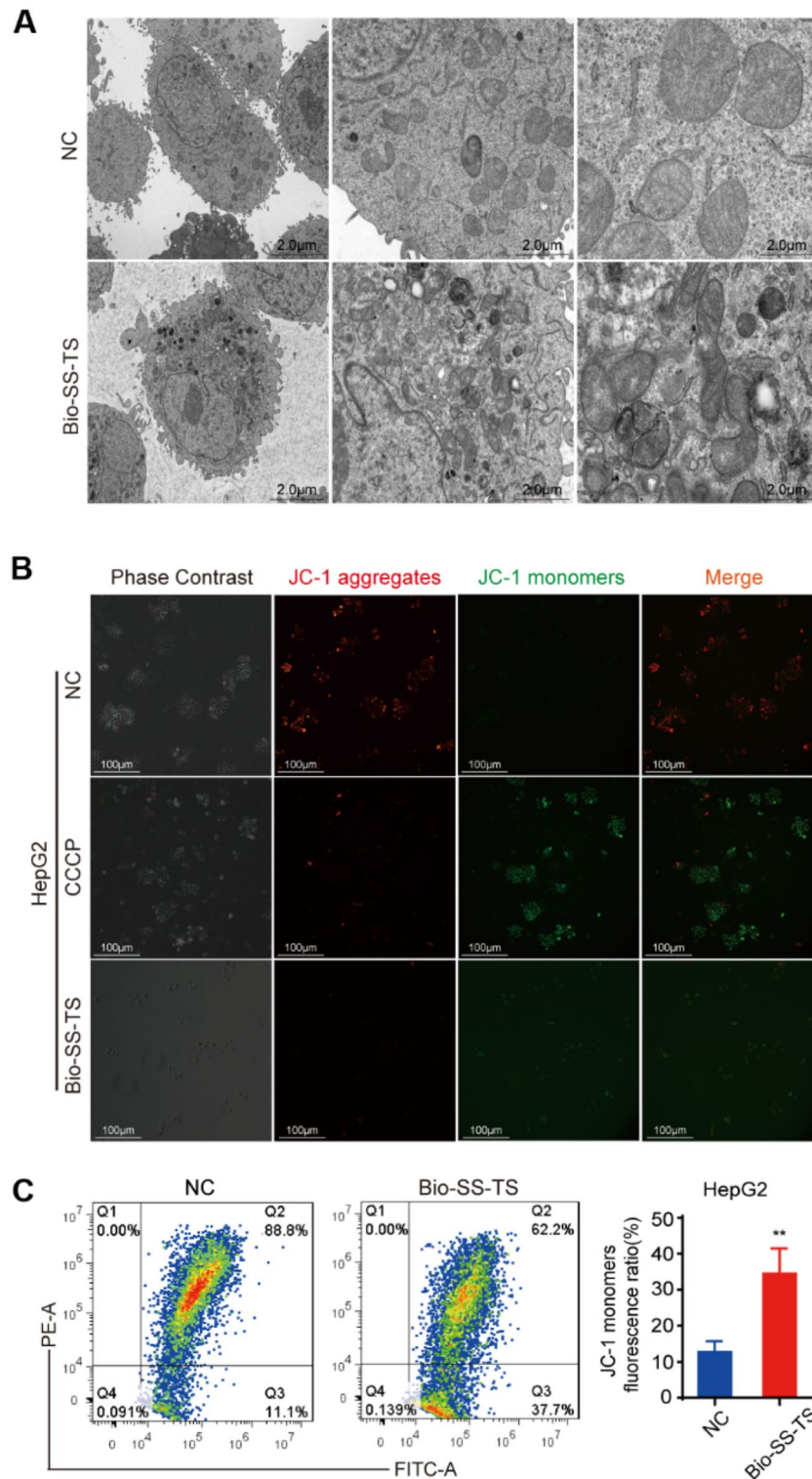


**Fig. 7** Effect of Bio-SS-TS on mitochondrial membrane potential in hepatoma cells. **A** The ultrastructure of HepG2 cells was detected by transmission electron microscopy. **B** The mitochondrial membrane potential of HepG2 cells was detected by optical microscopy. **C** The changes in mitochondrial membrane potential in HepG2 cells were detected by flow cytometry. \*\*  $P < 0.01$ . PS: CCCP is a mitochondrial electron transport chain inhibitor that can induce a decrease in mitochondrial membrane potential, and we used it as a positive control

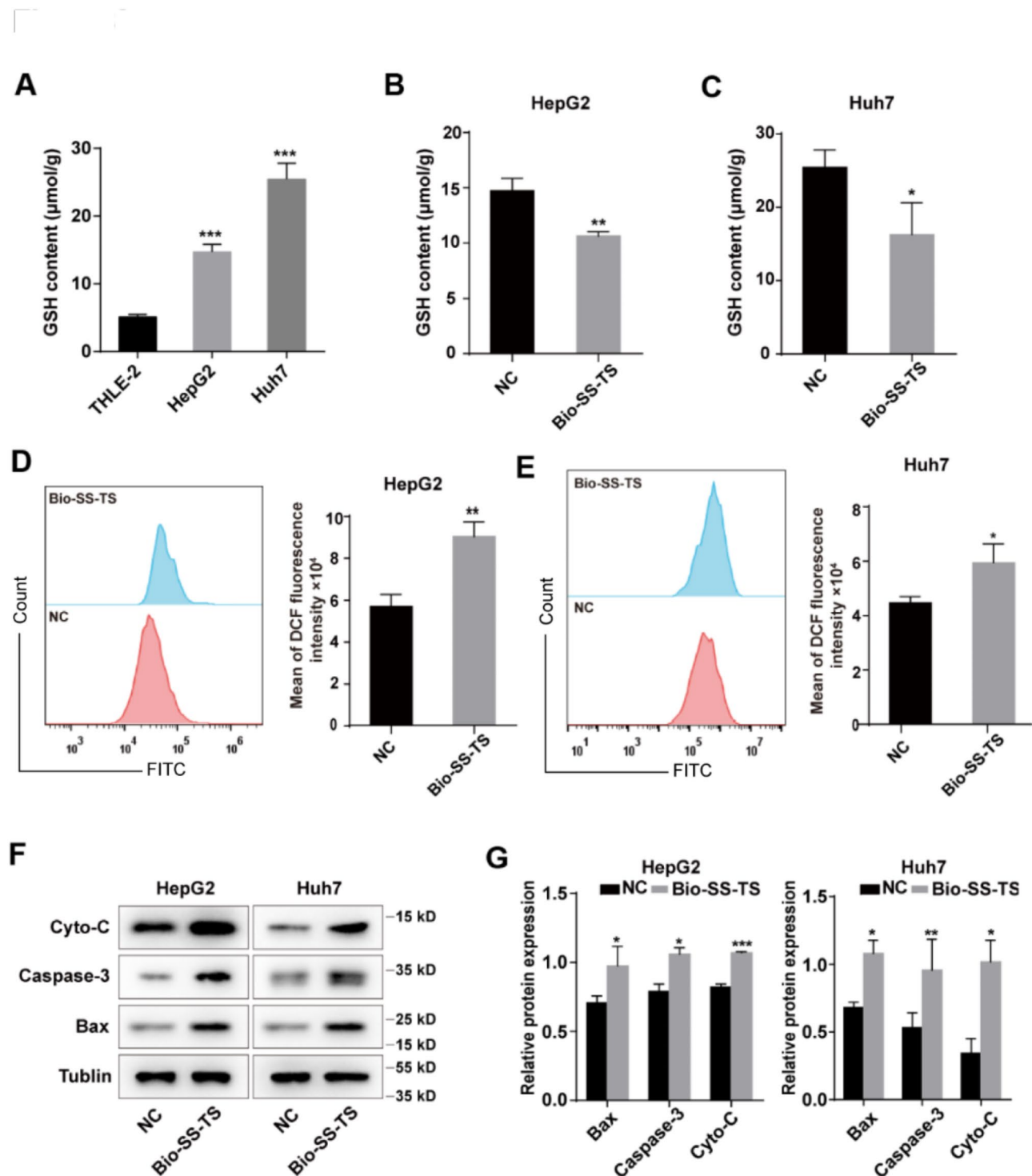


**Fig. 8** Bio-SS-TS Induces Apoptosis in Hepatoma Cells. **A** GSH content in THLE-2/HepG2/Huh7 cells. **B-C** Effect of Bio-SS-TS on GSH content in HepG2/Huh7 cells. **D-E** Reactive oxygen species (ROS) changes in HepG2/Huh7 cells treated with Bio-SS-TS for 72 h were detected. **F-G** The apoptosis-related protein expression in HepG2/Huh7 cells was detected after 72 h. \*  $P < 0.05$ ; \*\*  $P < 0.01$ ; \*\*\*  $P < 0.001$

## Discussion

Traditional medicine has long been used in the treatment of cancer [24, 25], and dandelion, a classical Chinese herbal medicine, has exhibited antitumor efficacy

[10, 26]. However, the molecular mechanisms underlying this antitumor activity remain to be fully understood, which limits its application. TS, a natural product extracted from dandelion [27], has been shown to exert

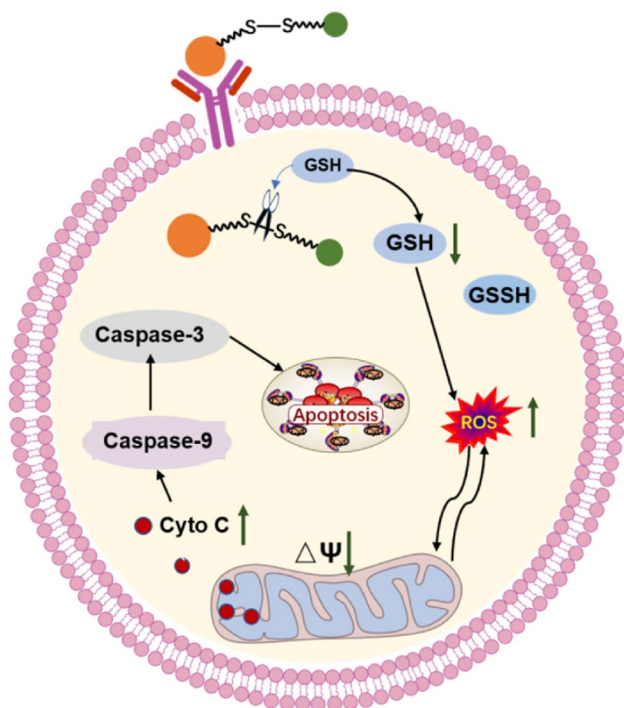


**Fig. 9** Mechanism of Action of Bio-SS-TS Against LC. After the structure of dandelion sterol modified by the biotin disulfide bond enters the cell membrane, the disulfide bond is broken under reduced glutathione, releasing dandelion sterol, which exerts an anti-liver cancer effect. Due to the decrease in reduced glutathione, the release of reactive oxygen species in mitochondria increases, decreasing mitochondrial membrane potential and increasing membrane permeability. A large amount of cytochrome C is released into the cell, which activates caspase-9 and further activates downstream caspase-3, producing a cascade of Caspase reactions and causing apoptosis

anti-growth effects against liver cancer cells [28]. The present study modified TS by conjugating biotin, a protein that targets tumors via its receptor on cancer cell surface, to TS using a disulfide linker to generate a new molecule known as Bio-SS-TS. As demonstrated in the present study, this novel compound exhibited high efficacy in inhibiting liver cancer cell proliferation. The prodrug Bio-SS-TS provides a potent new strategy for specific tumor-targeted therapy. In addition, Bio-SS-TS prevented tumor growth by disrupting mitochondria-dependent apoptosis (Fig. 9).

We previously found that TS caused tumor cells to undergo apoptosis, which attracted a large number of CD4<sup>+</sup> and CD8<sup>+</sup> T-lymphocytes into tumor tissues [15]. Furthermore, in tumor-bearing mice, the immune response was significantly enhanced when TS suppressed the production of STAT3 protein in T-cells, enhancing the anticancer effect of T-cells [15]. However, the efficacy of TS in the treatment of cancers is limited due to its poor solubility and lack of tumor selectivity. After conducting a thorough literature review, the present study synthesized a novel prodrug, Bio-SS-TS, by linking biotin

and disulfide bonds on TS to address the aforementioned issue. It is envisaged that using such a cutting-edge prodrug can increase drug accumulation in tumor tissues, thereby increasing the efficacy of tumor inhibition, and may provide patients with cancer with a more potent therapeutic option.

The present study evaluated the safety of Bio-SS-TS in mice by measuring the serum levels of ALT, AST, BUN and SCR. The results suggested that Bio-SS-TS was relatively safe for use in vivo, which may be attributed to its optimized structure. Notably, to the best of our knowledge, the present study demonstrated, for the first time, that treatment with Bio-SS-TS impaired mitochondrial membrane integrity, and also caused a considerable increase in ROS generation, which potentially helps to justify the more potent antitumor effects. However, Lu et al. [29] revealed that in non-small cell lung cancer, TS did not affect the ROS levels. Therefore, this may be a unique mechanism of Bio-SS-TS in liver cancer. Intracellular GSH levels are crucial for maintaining the redox balance within the cell by clearing free radicals and peroxide. The results of the present study indicated that the GSH content in liver cancer cells was significantly reduced following treatment with Bio-SS-TS due to the cleavage of disulfide bonds in Bio-SS-TS, which consumes GSH substantially; GSH depletion causes ROS to accumulate in the mitochondria, which damages cells and encourages apoptosis.

The capacity of biotin molecules or biotin conjugates to selectively target cancer cells is well recognized [30, 31]. Maiti et al. [32] designed a cancer-targeting unit by combining gemcitabine, a cleavable disulfide link unique to thiols, and biotin, a cancer-targeting unit. Udompholkul et al. [33] developed EphA2-agonist-biotin-streptavidin conjugates to enhance the agonistic activity of EphA2-targeting ligands. In the present study, it was discovered that Bio-SS-TS significantly outperformed TS in vitro in inducing the apoptosis of hepatoma cells, which may be related to the improved targeted efficacy of the biotin molecule.

## Conclusions

In conclusion, the present study revealed a novel method by which Bio-SS-TS exerts its improved anticancer effects, thus demonstrating the potential clinical use of the drug. This approach can potentially deliver potent tumor-targeting drugs to tumor tissues to kill cancer cells in patients with liver cancer. Recently, Zhao et al. [34] revealed that TS suppressed gastric cancer progression by inhibiting GPD2-mediated glycolysis, suggesting a novel mechanism of TS. However, further investigations are warranted to explore the possible effects of glycometabolism, which could broaden the therapeutic potential of the drug. The present study reveals a novel method by

which Bio-SS-TS exerts its improved anticancer effects, thus paving the way for the potential clinical use of the drug.

### Supplementary Information

The online version contains supplementary material available at <https://doi.org/10.1186/s12575-025-00272-7>.

#### Supplementary Material 1

Supplementary Material 2: Fig. S1 The effect of Bio-SS-TS on the CD4+ and CD8 T+ lymphocytes infiltration in tumor tissue. Fig. S2 The effects of Bio-SS-TS on the heart, brain, and lung of Kunming mice were examined using H&E staining. Fig. S3 Effect of Bio-SS-TS on mitochondrial membrane potential in Huh7 cells. A The mitochondrial membrane potential of Huh7 cells was detected by optical microscopy. B The changes in mitochondrial membrane potential in Huh7 cells were detected by flow cytometry. \*Compared with the control group,  $P < 0.05$ ; \*\*Compared with control group,  $P < 0.01$ ; \*\*\*Compared with control group,  $P < 0.001$ .

### Acknowledgements

We thank Dr Linhua Jiang for his help in the revision of the manuscript.

### Author Contributions

JL, HJ and FR designed the study; YQ, JS, HC, ML, YL, BL, PZ, TZ, GW, CG and YZ carried out experiments and analyzed data. The final manuscript was approved by all authors.

### Funding

This work was supported by the Key Research and Development Project of Henan Province (231111311300); the Technological Projects of Henan Province (232102310070); the Key Scientific Research Projects of Universities in Henan Province (24A310013); and the Joint Fund of the Henan Science and Technology Research and Development Program (245101610006).

### Data Availability

No datasets were generated or analysed during the current study.

### Declarations

#### Ethics Approval and Consent to Participate

The Xinxiang Medical University Ethics Committee has approved the in vivo experiments. (approval no. 20210489, Xinxiang, Henan, China).

#### Consent for Publication

Not applicable.

#### Competing Interests

The authors declare no competing interests.

Received: 16 December 2024 / Accepted: 28 February 2025

Published online: 28 March 2025

### References

- Wang H, Chu F, Zhijie L, Bi Q, Lixin L, Zhuang Y, et al. MTBP enhances the activation of transcription factor ETS-1 and promotes the proliferation of hepatocellular carcinoma cells. *Front Oncol*. 2022;12:985082.
- Geh D, Leslie J, Rumney R, Reeves HL, Bird TG, Mann DA. Neutrophils as potential therapeutic targets in hepatocellular carcinoma. *Nat Rev Gastroenterol Hepatol*. 2022;19:257–73.
- Xiao Z, Chung H, Banan B, Manning PT, Ott KC, Lin S, et al. Antibody mediated therapy targeting CD47 inhibits tumor progression of hepatocellular carcinoma. *Cancer Lett*. 2015;360:302–9.
- Thomas MB, Jaffe D, Choti MM, Belghiti J, Curley S, Fong Y, et al. Hepatocellular carcinoma: consensus recommendations of the National Cancer Institute clinical trials planning meeting. *J Clin Oncol: Official J Am Soc Clin Oncol*. 2010;28:3994–4005.
- Vogel A, Meyer T, Sapisochin G, Salem R, Saborowski A. Hepatocellular carcinoma. *Lancet*. 2022;400:1345–62.
- Luo XY, Wu KM, He XX. Advances in drug development for hepatocellular carcinoma: clinical trials and potential therapeutic targets. *J Exp Clin Cancer Res*. 2021;40:172.
- Petrowsky H, Fritsch R, Guckenberger M, De Oliveira ML, Dutkowsky P, Clavien PA. Modern therapeutic approaches for the treatment of malignant liver tumours. *Nat Rev Gastroenterol Hepatol*. 2020;17:755–72.
- Xiao J, Xing F, Liu Y, Lv Y, Wang X, Ling MT, et al. Garlic-derived compound S-allylmercaptocysteine inhibits hepatocarcinogenesis through targeting LRP6/Wnt pathway. *Acta Pharm Sin B*. 2018;8:575–86.
- Hui F, Qin X, Zhang Q, Li R, Liu M, Ren T, et al. Alpinia oxyphylla oil induces apoptosis of hepatocellular carcinoma cells via PI3K/Akt pathway in vitro and in vivo. *Biomed Pharmacother*. 2019;109:2365–74.
- Deng XX, Jiao YN, Hao HF, Xue D, Bai CC, Han SY. Taraxacum Mongolicum extract inhibited malignant phenotype of triple-negative breast cancer cells in tumor-associated macrophages microenvironment through suppressing IL-10 / STAT3 / PD-L1 signaling pathways. *J Ethnopharmacol*. 2021;274:113978.
- Saratale RG, Benelli G, Kumar G, Kim DS, Saratale GD. Bio-fabrication of silver nanoparticles using the leaf extract of an ancient herbal medicine, dandelion (*Taraxacum officinale*), evaluation of their antioxidant, anticancer potential, and antimicrobial activity against phytopathogens. *Environ Sci Pollut Res Int*. 2018;25:10392–406.
- Chen J, Wu W, Zhang M, Chen C. Taraxasterol suppresses inflammation in IL-1 $\beta$ -induced rheumatoid arthritis fibroblast-like synoviocytes and rheumatoid arthritis progression in mice. *Int Immunopharmacol*. 2019;70:274–83.
- Schutz K, Carle R, Schieber A. Taraxacum—a review on its phytochemical and pharmacological profile. *J Ethnopharmacol*. 2006;107:313–23.
- Liu W, Yu Q, Wang F, Li Y, Zhang G, Tao S. Taraxasterol attenuates melanoma progression via inactivation of reactive oxygen species-mediated PI3K/Akt signaling pathway. *Hum Exp Toxicol*. 2022;41:9603271211069034.
- Ren F, Zhang Y, Qin Y, Shang J, Wang Y, Wei P, et al. Taraxasterol prompted the anti-tumor effect in mice burdened hepatocellular carcinoma by regulating T lymphocytes. *Cell Death Discovery*. 2022;8:264.
- Sadat Abolmaali S, Zarenejad S, Mohebi Y, Najafi H, Javanmardi S, Abedi M, et al. Biotin receptor-targeting nanogels loaded with methotrexate for enhanced antitumor efficacy in triple-negative breast cancer in vitro and in vivo models. *Int J Pharm*. 2022;624:122049.
- Li K, Dong W, Liu Q, Lv G, Xie M, Sun X, et al. A biotin receptor-targeted silicon(IV) phthalocyanine for in vivo tumor imaging and photodynamic therapy. *J Photochem Photobiol B*. 2019;190:1–7.
- Lee MH, Yang Z, Lim CW, Lee YH, Dongbang S, Kang C, et al. Disulfide-cleavage-triggered chemosensors and their biological applications. *Chem Rev*. 2013;113:5071–109.
- Li R, Xiong YL. Disulfide cleavage to improve interfacial behavior and emulsification properties of oat protein. *Food Chem*. 2022;404:134511.
- Zeng F, Yang C, Gao X, Li X, Zhang Z, Gong R. Comprehensive Elucidation of the structural and functional roles of engineered disulfide bonds in antibody Fc fragment. *J Biol Chem*. 2018;293:19127–35.
- Jaganjac M, Milkovic L, Sunjic SB, Zarkovic N. The NRF2, thioredoxin, and glutathione system in tumorigenesis and anticancer therapies. *Antioxid (Basel)*. 2020;9.
- Lee MH, Sessler JL, Kim JS. Disulfide-based multifunctional conjugates for targeted theranostic drug delivery. *Acc Chem Res*. 2015;48:2935–46.
- Cheng X, Xu HD, Ran HH, Liang G, Wu FG. Glutathione-Depleting nanomedicines for synergistic Cancer therapy. *ACS Nano*. 2021;15:8039–68.
- Zhang Y, Wei Y, Jiang S, Dang Y, Yang Y, Zuo W, et al. Traditional Chinese medicine CFF-1 exerts a potent anti-tumor immunity to hinder tumor growth and metastasis in prostate cancer through EGFR/JAK1/STAT3 pathway to inhibit PD-1/PD-L1 checkpoint signaling. *Phytomedicine: Int J Phytotherapy Phytomedicine*. 2022;99:153939.
- Wang Y, Zhang X, Wang Y, Zhao W, Li H, Zhang L, et al. Application of immune checkpoint targets in the anti-tumor novel drugs and traditional Chinese medicine development. *Acta Pharm Sinica B*. 2021;11:2957–72.
- Qu J, Ke F, Yang X, Wang Y, Xu H, Li Q, et al. Induction of P-glycoprotein expression by dandelion in tumor and heart tissues: impact on the anti-tumor activity and cardiotoxicity of doxorubicin. *Phytomedicine*. 2022;104:154275.

27. Xu L, Yu Y, Sang R, Li J, Ge B, Zhang X. Protective effects of taraxasterol against Ethanol-Induced liver injury by regulating CYP2E1/Nrf2/HO-1 and NF-kappaB signaling pathways in mice. *Oxid Med Cell Longev*. 2018;2018:8284107.
28. Bao T, Ke Y, Wang Y, Wang W, Li Y, Wang Y, et al. Taraxasterol suppresses the growth of human liver cancer by upregulating Hint1 expression. *J Mol Med (Berl)*. 2018;96:661–72.
29. Lu J, Shuai B, Shou Z, Guo W, Zhou C, Ouyang X et al. Taraxasterol inhibits tumor growth by inducing apoptosis and modulating the tumor microenvironment in Non-Small cell lung Cancer. *Cancers*. 2022;14.
30. Liu W, Ma X, Jin Y, Zhang J, Li Y, Tang Y et al. Chlorin e6-Biotin conjugates for Tumor-Targeting photodynamic therapy. *Molecules*. 2021;26.
31. Maiti S, Paira P. Biotin conjugated organic molecules and proteins for cancer therapy: A review. *Eur J Med Chem*. 2018;145:206–23.
32. Maiti S, Park N, Han JH, Jeon HM, Lee JH, Bhuniya S, et al. Gemcitabine-coumarin-biotin conjugates: a target specific theranostic anticancer prodrug. *J Am Chem Soc*. 2013;135:4567–72.
33. Udompholkul P, Baggio C, Gambini L, Sun Y, Zhao M, Hoffman RM et al. Effective tumor targeting by EphA2-Agonist-Biotin-Streptavidin conjugates. *Molecules*. 2021;26.
34. Zhao Y, Zhang L, Guo M, Yang H. Taraxasterol suppresses cell proliferation and boosts cell apoptosis via inhibiting GPD2-mediated Glycolysis in gastric cancer. *Cytotechnology*. 2021;73:815–25.

### Publisher's Note

Springer Nature remains neutral with regard to jurisdictional claims in published maps and institutional affiliations.